

NONLINEAR PHASE SPEEDS AND DEPTH INVERSIONS

Patricio Catalán¹ and Merrick C. Haller²

¹ Ocean Engineering Program, Department of Civil, Construction and Environmental Engineering, 202 Apperson Hall, Oregon State University, Corvallis, OR. catalapa@enr.orst.edu.

² Ocean Engineering Program, Oregon State University. hallerm@enr.orst.edu

Abstract: Experiments were conducted in a laboratory facility under with a fixed bathymetric profile containing a single bar. A hybrid data set was collected consisting of remotely sensed wave data combined with model-generated wave amplitude profiles. The data is used to test the improvements in depth retrieval through the use of a nonlinear composite dispersion that is applicable in arbitrary water depths. The dispersion relation relates the wave properties with the local water depth and the results suggest that inclusion of nonlinearity improves depth estimation on shallow water.

INTRODUCTION

The characterization of bathymetry and its time evolution is very important for both oceanographic science applications and for societal reasons relating to coastal engineering and development. Historically, the process of depth surveying has been costly and labor-intensive, and often dangerous. Bathymetry is especially important in the nearshore region; hence, a method that is both economic and reliable is of great interest. In this regard, depth inversion techniques take advantage of the interaction between the surface wave field and the underlying bathymetry such that observations of surface wave propagation can be coupled with a dispersion relation to infer bathymetry. Using field measurements, several different types of observed wave data have been tested in inversion methods, e.g. arrays of pressure sensors (Holland 2001), marine radar (Bell 1999), aerial photogrammetry (e.g. Dugan and Piotrowsky 2002)) and video imagery (Stockdon and Holman 2000). Remote sensing techniques appear to be more suitable than in situ measurements for depth inversion techniques, because they can provide truly synoptic data at a relatively low cost, without intrusion, and with good spatial resolution.

Typically, these studies use the linear wave dispersion relation given in Eq. 1,

$$c^2 = g / k \tanh(kh), \quad (1)$$

which can be solved explicitly in terms of measured wave phase speeds (c) and wavenumber (k) to perform the inversion to retrieve depths (h). Agreement is generally good in intermediate water depths in the absence of currents, where relative errors are of order 10%. However, errors tend to increase as waves enter shallow water, where typically depths are overpredicted. This is the result of the observed speeds being larger than those predicted by the linear dispersion relation, and errors of more than 25% are not uncommon. In shallow water, the errors have shown to be correlated with wave height (Stockdon and Holman 2000; Holland 2001). Holland (2001) used a correction for the shallow water approximation of Eq. 1 in the form of the phase speed of cnoidal waves

$$c = \sqrt{g(h + \alpha H_s)}, \quad (2)$$

but applied only a single offshore value of wave height across the profile. He used a value of $\alpha \sim 0.4-0.5$ and reduced the shallow water errors to the degree of accuracy of linear inversions in intermediate water. Errors have also been shown to increase in the shoaling region prior to breaking (e.g. Grilli 1998; Stockdon and Holman 2000), suggesting that the observed differences in shallow water and shoaling region can be accounted for by including nonlinear effects in the inversion algorithm. In addition to field based depth inversions, numerically simulated free surface maps have been used to test inversion algorithms, in some cases using models that account for many nonlinear processes (e.g. Grilli 1998; Kennedy et al 2000; Misra et al 2003). These nonlinear methods can potentially lead to improved depth estimates; however, they have only been tested with synthetic data. The main reason for this is that free surface elevation data is required, or at least dense profiles of wave height. The current status of the remote sensing methods is such that they can only provide a fraction of the required information to perform nonlinear depth inversions, therefore the extra parameters must be sought elsewhere. It is of interest nevertheless to study how nonlinear depth inversions perform when used with actual wave data.

In this study, we undertake a novel approach for investigating phase speeds of nonlinear waves and the potential for using them for depth inversions. The approach is novel in the sense that our observational data set consists of both in situ and remotely sensed data combined with high resolution numerical data for interpolating between the in situ measurements. The resulting hybrid data set provides the required wave parameters with a high resolution to test nonlinear depth inversions.

METHODOLOGY

Nonlinearity is included in the depth inversion algorithm by means of the composite dispersion relation proposed by Kirby and Dalrymple (1986), which is essentially an empirical combination of different nonlinear theories dependent upon the relative water depth. Intermediate to deep water waves are modeled using a third order Stokes theory, resulting from a series expansion of wave parameters under the assumption of smallness of the parameter $\varepsilon=k|A|$, where k is the wavenumber and $A=H/2$ is the wave amplitude. Considering that this formulation has limitations in shallow water, the empirical model of Hedges (1976) is used in this region instead. The asymptotic behavior of the two is matched by the following dispersion relation (Kirby and Dalrymple 1986)

$$\frac{c}{c_0} = (1 + f_1 \varepsilon^2 D) \tanh(kh + f_2 \varepsilon), \quad (3)$$

$$f_1 = \tanh^5(kh), \quad (4)$$

$$f_2 = [kh / \sinh(kh)]^4, \quad (5)$$

$$D = \frac{\cosh(4kh) + 8 - \tanh^2(kh)}{8 \sinh^4(kh)} \quad (6)$$

The shallow water asymptote is $c = \sqrt{g(h+|A|)}$, which is essentially similar to Eq. (2) used by Holland (2001) in shallow water. Furthermore, the resulting monochromatic dispersion model given by Eq. (3) collapses to the linear dispersion for zero amplitude ($A=0$), thus allowing direct comparison with linear-based inverted depths when estimating the benefits of adding nonlinearity to the depth inversion algorithm.

However, usage of this model requires a detailed wave amplitude profile, which is not presently available from operational remote sensors. As a consequence, an indirect approach is used and the wave amplitude profiles are obtained using numerical modeling. There is a wide range of models that can provide the required wave amplitude profile, for instance the phase-averaged models of Thornton and Guza (1983), the REF/DIF1 model (Kirby and Dalrymple 1994), which solves combined refraction and diffraction by solving the Mild Slope Equation; or phase-resolving models based on the nonlinear Boussinesq equations (e.g. Schäffer et al 1993; Wei et al 1995; Lynnet et al 2002 and their extensions). Whichever the choice, it must be stressed that the model output is to be considered as a proxy of the possible output of future remote sensing systems. In particular, we use here the extension of the phase-resolving Boussinesq model first given in Wei et al (1995) and freely available as FUNWAVE (Kirby et al 1998). The model is calibrated with in situ data. In addition remote video data is used to estimate other wave parameters such as phase speed, wave frequency, and wavenumber.

EXPERIMENTS

Large scale laboratory experiments were performed in the Long Wave Flume (LWF) at the O.H. Hinsdale Wave Lab (Oregon State University). The usable length of this flume is approximately 90 m, and it is 3.7 m wide and 4.6 m deep. The flume has a flap-type wavemaker at one end with active wave absorption capabilities. The bottom of the flume

was configured into a piecewise continuous, barred profile designed to approximate the bar geometry of an observed field beach profile at a 1:3 reduction in scale; specifically, the October 11, 1994 profile of the DUCK94 field experiment (see Scott et al 2005).

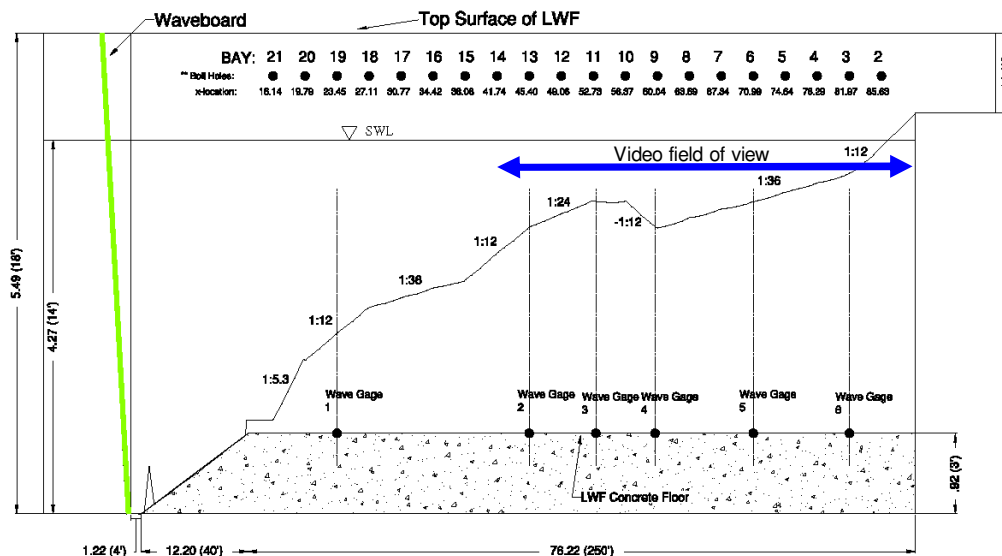


Figure 1: Experimental layout for the Long Wave Flume, including bathymetry, wave gage locations, bay numbers and video field of view.

The LWF coordinate system has the x -axis pointing onshore along the centerline with the origin at the wavemaker, and the water depth there was maintained at 4.27 m. There is an array of threaded inserts on each wall of the LWF that are spaced at 3.66 m and designed for instrument mounting. The location of these corresponds to the bay numbers also shown in Figure 1. Six resistance-type wave gages were used to measure free surface elevation and were sampled at 50 Hz. The wave gages were installed on the east wall of the tank at cross shore locations $x=23.45, 45.40, 52.73, 60.04, 70.99$ and 84.97 m (bays 19, 13, 11, 9, 6 and 3, respectively).

Video observations were collected using the new ARGUS III video station installed at the lab. This station is maintained by The Argus Program (Coastal Imaging Lab, COAS, OSU) and consists of three digital cameras mounted near the ceiling and aimed at different sections of the LWF. The field of view of the cameras spans offshore from bay 13 to the dry beach. Individual images (or a series of images) from each camera can be merged and rectified into a single snapshot as shown in Figure 2. Also, shown in the figure are the locations of five of the six in-situ wave gages. The sixth gage is offshore of the field of view.

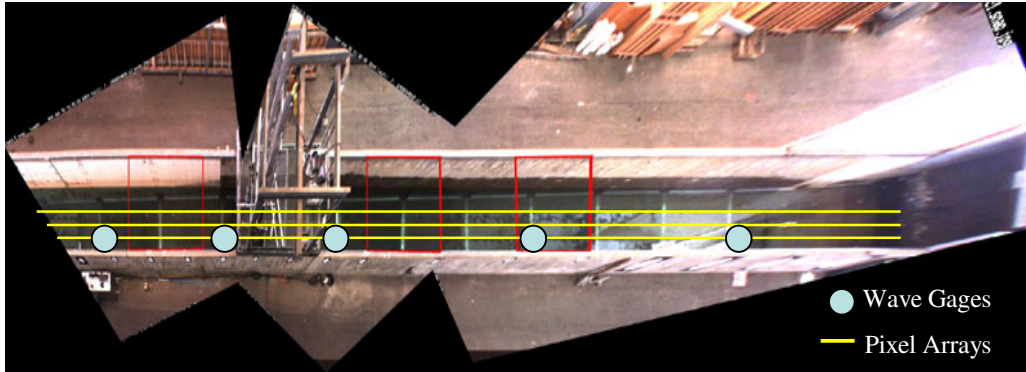


Figure 2: Field of view from the video cameras, pixel arrays shown by yellow lines, wave gages by circles.

We only sampled three different pixel arrays indicated by the yellow lines in Figure 2. These arrays spanned $41.7 < x < 100$ m at longshore coordinates $y = -1.2, 0$ and 0.6 m and were sampled at 10 Hz. After interpolation to a uniform grid, there were a total of 5836 pixels in each array with a Δx of 1 cm. The wave conditions in the tank were essentially uniform in the y -direction (longshore), however, the lighting conditions were not. We restricted our analysis to the pixel array that was least degraded by the ambient lighting conditions, specifically array $y = -1.2$ m.

The total data set consists of 10 separate wave conditions, including 6 regular and 4 random wave conditions. For this work we have only analyzed the regular wave conditions, which are listed in Table 1. Further details of the experimental procedure and video data processing can be found in Catalan (2005).

Table 1. Wave Conditions for Regular Wave Tests

Run #	T (sec)	H_0 (m)	H_b (m)	$(kh)_b$
35	2.7	0.62	0.66	0.66
36	4.0	0.79	0.75	0.43
37	5.0	0.81	0.81	0.34
38	6.0	0.66	0.70	0.28
39	8.0	0.62	0.74	0.21
40	4.0	0.59	0.56	0.43

Values are wave period (T), deep water wave height (H_0), breaking wave height H_b , relative water depth at break point $(kh)_b$

DATA ANALYSIS

Video data

Video data for a single pixel array is obtained in the form of video pixel intensity time-space maps (timestacks) of the recognizable wave signature. Although in video data from the field waves are often recognizable by different mechanisms like specular reflection of

light on the free surface or scattered reflection from the turbulent region associated with wave breaking, lighting conditions for this laboratory set up were amenable to the wave breaking related signature only, reducing the cross-shore distance available for inversions.

Pixel intensity spectra are obtained at cross-shore locations where the local variance is greater than the variance calculated over the entire image, thus locations with strong wave related signals are retained. Frequency at the spectral peak is obtained at each of these locations and averaged to obtain the representative frequency of the run. Results were typically within 1% of the input wave period shown on Table 1.

Estimation of phase speed is performed by a calculation of the slope of the trajectory of a characteristic point of the wave. The analysis is performed on a wave-by-wave basis, and results at each cross-shore location are averaged over the number of waves recorded, which was typically more than 50. Analysis of the pixel intensity time series showed that the wave front is characterized by a strong gradient in the pixel intensity signal that is easily identified. However, other features also exhibit a similar behavior, in particular the passage of foam left behind by the progressive wave. The speed of these foam patches is not related with the speed of the main wave, as can be seen on Figure 3. In order to clearly discriminate wave fronts from other features, edge detection tools are used to isolate individual waves, from where the front can be correctly identified. This process can be seen on Figure 3. The resulting phase speed profile is further smoothed by applying a low pass filter in the form of a double-sided 11 point spatial running average.

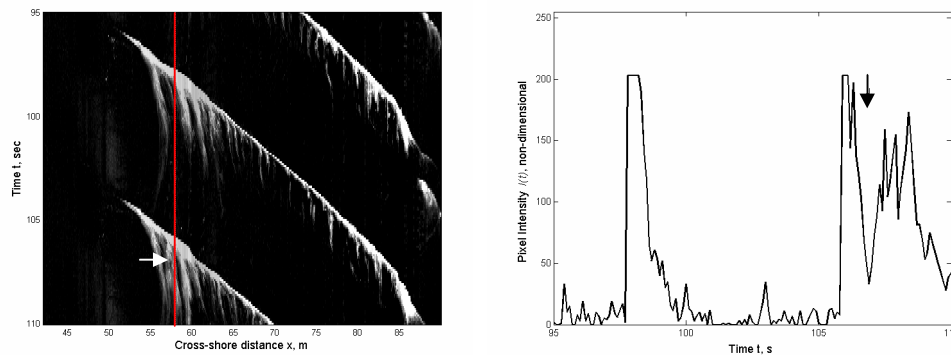


Figure 3: a) Intensity timestack for Run 39. Bright regions indicate presence of foam associated with breaking and orbital foam patches left behind by the progressive wave. b) Transect of the pixel intensity signal at $x=58$ m (red line on a)), where the wave front is clearly recognizable. Arrows indicate the persistent foam left behind by the wave.

By using these two procedures, two wave parameters (peak frequency f and phase speed c) are directly obtained from the video dataset, from which it is possible to estimate wavenumber as $k=2\pi f/c$. These parameters provide enough information to perform linear depth inversions.

Numerical model

The free surface time series from the six fixed wave gages are used to calibrate the Boussinesq model FUNWAVE. The model was driven by the measured free surface time series recorded at the offshore gage (bay 19, $x=23.45$ m). Calibration consisted of matching the wave height profile by adjusting model parameters related with the breaking formulation implemented in the model (Kennedy et al., 2000). Figure 5 shows an example of the wave height profile obtained after calibration. It can be seen that maximum wave heights were underpredicted over the bar, and overpredicted on the bar trough, a result common for all cases tested. However, due to the reduction on the domain induced by the video technique, our attention was focused on the behavior shoreward of the bar where a reasonable agreement was found for all cases.

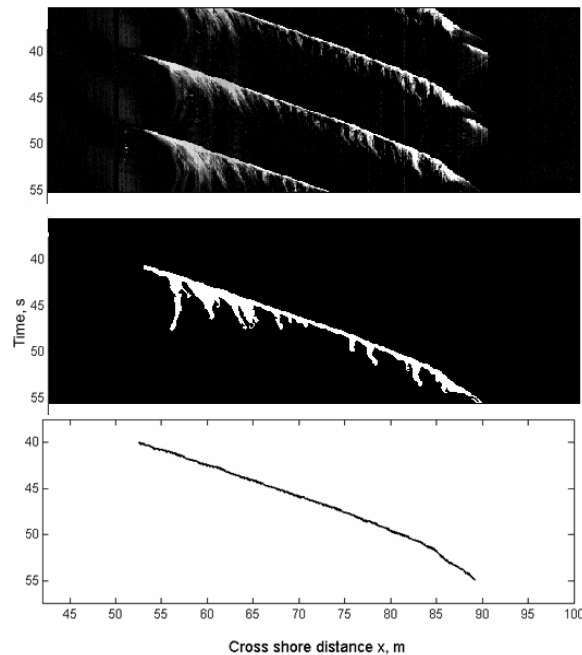


Figure 4: Example of front selection and tracking procedure a) Original timestack; b) binary image showing an isolated wave; c) wave front trajectory.

The resulting wave height profile consisted of 210 cross-shore points extending from $x=27.7$ to $x=80.2$ m, which is slightly offshore of the still water shoreline. The profiles have a resolution of $\Delta x=0.25$ m; thus, effectively providing a dense profile to perform nonlinear depth inversions.

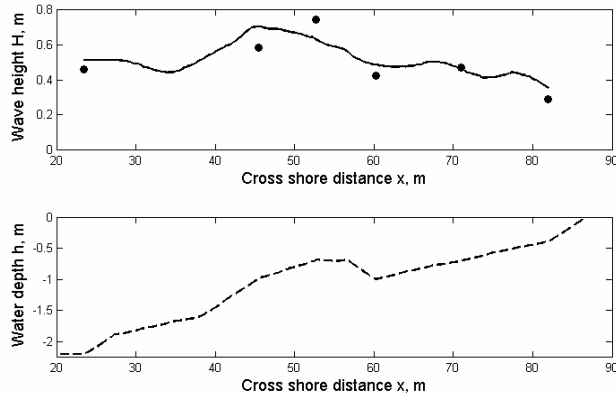


Figure 5: Example of numerical model results for a denser wave amplitude profile. In situ wave height data (circles), FUNWAVE wave heights (line) for Run 39.

RESULTS

Phase speeds

Figure 6 shows the result of the front tracking technique for Run 39, exhibiting some features common to all runs. Three regions can be recognized. First, offshore of the bar trough observed speeds are larger than those predicted by both dispersion models used, which eventually would result in a depth estimate showing a depression rather than a bar. This behavior can be initially explained in terms of bore growth and development.

The offshore increase in phase speed from zero value is related with the onset of breaking, which is observed by the camera by a sudden change in the pixel intensity signal, with a large slope for the front trajectory. Furthermore, as described by Basco (1985), as the roller develops it slides over the front face of the wave, thus effectively having an absolute speed larger than the carrier wave, until it reaches a stable position relative to the wave. This process can be observed in more detail in Figure 7. Once the roller is established, it is possible to identify a second region in which the front speed is bounded by both dispersion theories, but showing an overall tendency to be in closer agreement with the composite model. This region extends from the bar trough almost to the shoreline ($x=86.5$ m). Further onshore, a region of second breaking could be observed for some wave conditions where the steeper bathymetry induces wave shoaling and a secondary breaking, with another local process of roller growth. In this region it can also be observed that measured speeds are nonzero, whereas both theoretical models predict zero velocities. Clearly, one reason for this is use for the still water depth (h) rather than the setup corrected water depth ($h+\bar{\eta}$) when estimating the theoretical phase speed predicted by linear and composite dispersion models.

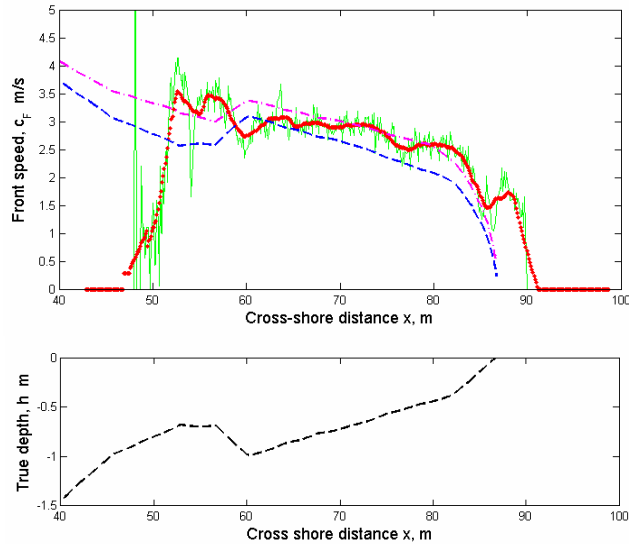


Figure 6: Example of result for the front tracking phase speed from Run 39, including raw (green) and phase averaged results (red circles). Also show are the theoretical estimates of phase speed obtained using linear (blue) and composite (magenta) dispersion relation.

Depth inversion

Five of the six cases listed on Table 1 are used for inversion, since Run 40 ($H=0.40$ m, $T=4.0$ s) exhibit a poor wave signal caused by cessation of breaking shoreward of the bar and for this reason is discarded. The remaining 5 cases provide individual depth profiles, but it is more convenient to present the analysis in terms of an average profile, which is obtained as the median of the individual estimates at each cross-shore location following Stockdon and Holman (2000). The resulting profile is shown on Figure 8. It can be seen that the bar trough system is not well retrieved by the current data set, but this is a direct consequence of the observed speed profile affected by the bore growth, a process that is not accounted for the theoretical models used. Shoreward of the bar trough, it can be seen that the nonlinear depth inversion provides better agreement than the linear case, with agreement getting better closer to the shore up to $x=80$ m. Shoreward of this point both models seem to diverge from the true depth.

In order to quantify the agreement, the dimensional difference error $D=h-h_{\text{true}}$ m and the relative error $R=D/h_{\text{true}}*100$ % are computed at each location, and the mean and root mean square of these estimates are obtained for the overall profile. The definition of the error is such that positive values indicate depth overprediction. When the bar is included, the mean relative error for the linear inversion is 43% (57% RMS) while for the nonlinear inversion these are reduced to 10% (24% RMS). Reducing depth estimation to the region where phase speed estimates appear to be more reliable ($60 \text{ m} < x < 80.2$), the mean relative error is reduced to 31 % (20% RMS) for the linear model and to -1.2% (10% RMS) for the nonlinear model. It should be noted that use of mean values for the

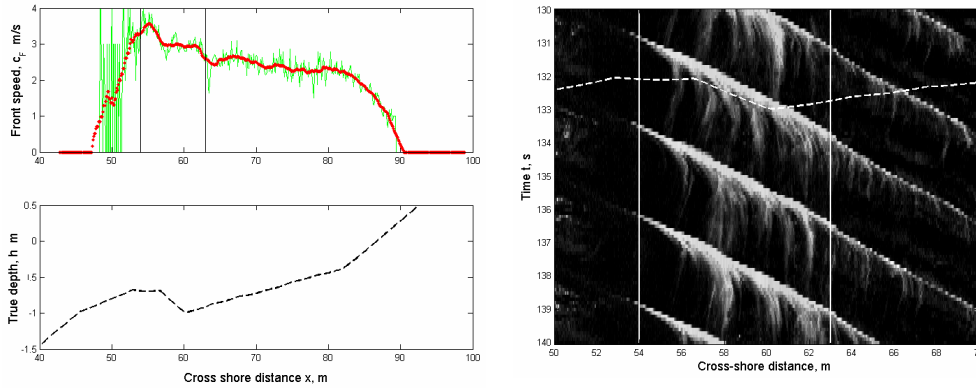


Figure 7: Phase speed associated with bore growth for run 35 a) Front tracking phase speed b) Pixel intensity timestack. Vertical lines denote the beginning of bore growth and its establishment relative to the wave. Steep gradients on the slope of the front trajectory can be noticed in this region.

error is subject to cancellation of values of the same magnitude but different sign, thus is considered that RMS values are a more reliable error measure. In consequence, it can be seen that relative errors (RMS) are reduced from $O(20\%)$ to $O(10\%)$ by using the nonlinear model. The relative depths covered by this subset of the domain covers from $0.11 < kh < 0.65$, thus the use of the full composite model is preferable over a simpler shallow water approximation such as Eq. (2) because the relative water depths are not known beforehand.

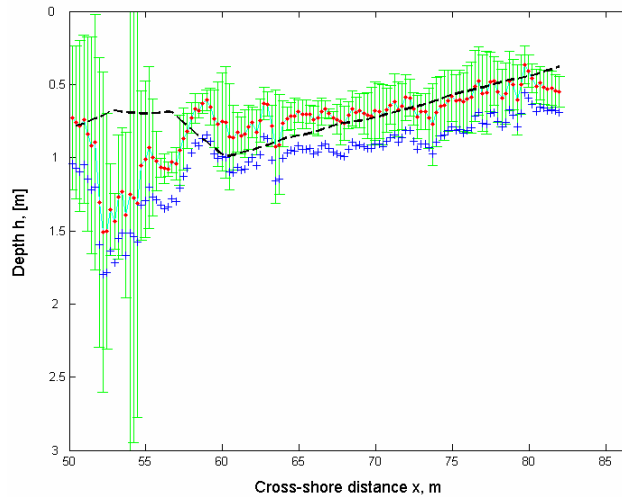


Figure 8: Averaged (median) depth profile obtained using linear (blue pluses) and nonlinear depth inversions (red dots), compared with true bathymetry (dashed black). Error bars (green) correspond to one standard deviation for the nonlinear profile.

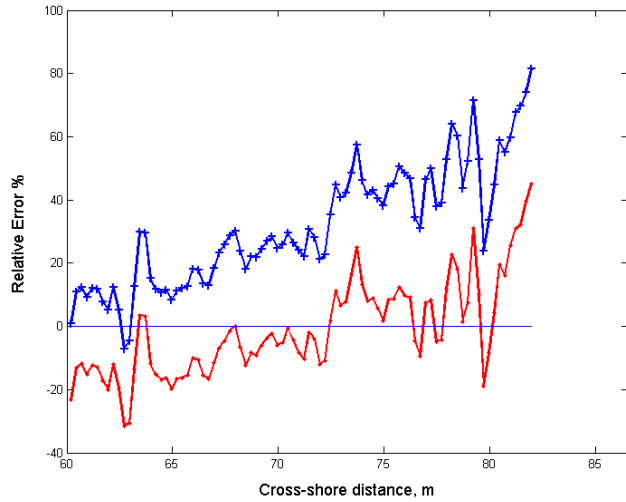


Figure 9: Relative error profile for linear (blue pluses) and nonlinear depth inversions (red dots).

Figure 9 shows the relative error profile, where the relative error shows a linear trend (increasing) as we progress onshore. Closer to the shoreline the error seems to increase abruptly, possible related with division by a small number as $h_{\text{true}} \rightarrow 0$. In order to isolate this numerical dependency, the relative error is analyzed versus the nonlinearity parameter $\delta=A/h_{\text{true}}$ and results shown on Figure 10, from where it can be observed that linear depth inversions exhibit a tendency to increase error with nonlinearity. On the other hand, nonlinear inversions appear to be less dependant on nonlinearity, but are biased.

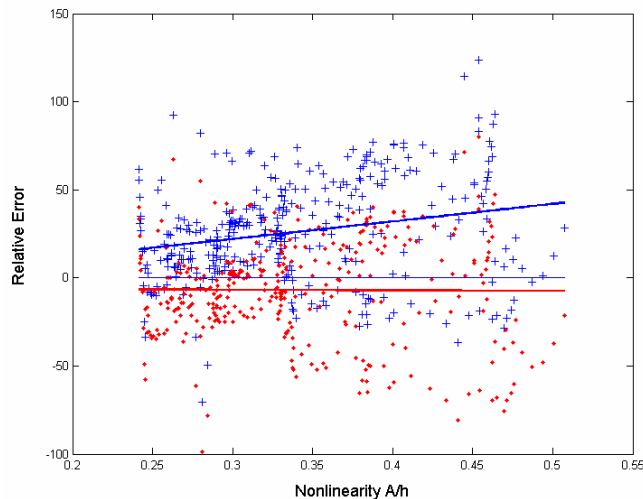


Figure 10: Relative error versus the nonlinearity parameter $\delta=A/h_{\text{true}}$ for linear (pluses) and nonlinear (red circles) depth inversions. Lines represent the

CONCLUSIONS

The main objective of the present study was to test a nonlinear model for the retrieval of depths using actual remotely sensed data. Nonlinearity was introduced by means of a simple dispersion equation that required only one extra parameter (wave height) as input and allowed direct comparison of the improvements of the nonlinear technique over traditional depth inversion methods based on the linear dispersion relation.

Results showed improved depth retrievals in shallow water, where errors for the average profile were reduced from 25% to 5% after inclusion of nonlinearity. Thus, inclusion of nonlinearity allowed shallow water estimates to have the same degree of accuracy obtained by previous studies in intermediate water using linear dispersion. In addition, the model tested introduces nonlinearity by means of a wave amplitude profile. Although the source for this parameter for the present study was numerical simulations calibrated with in situ measurements, we do not consider this as a limitation of the model. Instead, numerical simulations were here used as a proxy for a remotely sensed wave amplitude profile. It is expected that future developments of in remote sensing will allow this parameter to be estimated with more ease than free surface maps required by other more complex inversion techniques. If all the variables are measured remotely, nonlinear depth inversion has the additional advantage that it does not require calibration constants, hence its applicability would be straight forward.

The experimental set up used consisted of a barred beach, whose overall shape (i.e. the barred portion) was not recovered using the present algorithm. However, we note that the conditions tested were particularly difficult for both the depth inversion model and for video remote sensing. Notably, wave breaking began over the bar crest or just shoreward, and it is well known that optical signals exhibit a phase change in their relationship to the underlying waves at the break point, which considerably complicates the extraction of wave parameters in this region. Second, the simulated bar and trough were somewhat narrow with respect to the wavelength of the waves, which may indicate that the waves were not always in equilibrium with their local depth and will affect the ability of the dispersion relation to describe the local phase speed.

Finally, we conclude that the inversion algorithm shows promise as an improvement over linear inversion techniques. However, the depth inversion problem is fairly difficult and has a number of possible sources of error. Clearly, the over all accuracy of depth retrievals from inversion methods are decreased from traditional surveying methods; however, the cost savings and improvements in the speed of depth acquisition will still make inversion techniques useful in many situations, especially in areas with more smoothly varying profiles.

ACKNOWLEDGEMENTS

The authors wish to thank the staff at the O.H. Hinsdale Wave Research Lab for their support, including Dan Cox, Tim Maddux, Chris Scott and Terry Dibble. We are in debt with the Coastal Imaging Lab staff (Rob Holman, John Stanley, Jason Killian and Dan

Clark) and their ARGUS video system, which provided the fundamental data for this research.

REFERENCES

- Basco, D.R. (1985), "A qualitative description of wave breaking", *Journal of Waterway, Port, Coastal and Ocean Engineering* **111**(2), 171-188.
- Bell, P.S. (1999), "Shallow water bathymetry derived from an analysis of X-band marine radar images", *Coastal Engineering* **37**, 513-527.
- Catalan, P. (2005), "Hybrid approach to estimating bathymetry using remote sensing", M.Oc.E. thesis, Oregon State University.
- Dugan, J.P.; Piotrowski, C.C. & Williams, J. (2001), "Water depth and surface current retrievals from airborne optical measurements of surface gravity dispersion", *Journal of Geophysical Research* **106**(C8), 16903-16915.
- Grilli, S.T. (1998), "Depth inversion in shallow water based on nonlinear properties of shoaling periodic waves", *Coastal Engineering* **35**, 185-209.
- Hedges, T. (1976), "An empirical modification to linear wave theory", *Proc. Instn. Civ. Engrs.* **61**(Part 2), 575-579.
- Holland, T.K. (2001), "Application of the linear dispersion relation with respect to depth inversion and remotely sensed imagery", *IEEE Transactions on Geoscience and Remote Sensing* **39**(11), 2060-2071.
- Kennedy, A.B.; Dalrymple, R.A.; Kirby, J.T. & Chen, Q. (2000), "Determination of inverse depth using direct Boussinesq modeling", *Journal of Waterway, Port, Coastal, and Ocean Engineering* **126**(4), 206-214.
- Kirby, J.T. & Dalrymple, R.A. (1986), "An approximate model for nonlinear dispersion in monochromatic wave propagation models", *Coastal Engineering* **9**, 545-561.
- Kirby, J.T.; Wei, G.; Chen, Q.; Kennedy, A.B. & Dalrymple, R.A. (1998), "FUNWAVE 1.0 Fully nonlinear Boussinesq wave model. Documentation and User's manual"(CACR-98-06), Technical report, Center for Applied Coastal Research, Ocean Engineering Laboratory, University of Delaware.
- Kirby, J.T. & Dalrymple, R.A. (1994), "Combined Refraction / Diffraction Model REF/DIF1, Version 2.5 . Documentation and User's manual"(CACR-94-22), Technical report, Center for Applied Coastal Research, Ocean Engineering Laboratory, University of Delaware.
- Lynnet, P.J.; Wu, T. & Liu, P.L. (2002), "Modeling wave runup with depth integrated equations", *Coastal Engineering* **46**, 89-107.
- Madsen, P.; Sørensen, O. & H.A.Schäffer (1997), "Surf zone dynamics simulated by a Boussinesq type model.Part I. Model description and cross-shore motion of regular waves", *Coastal Engineering* **32**, 255-287
- Misra, S.K.; Kennedy, A.B. & Kirby, J.T. (2003), "An approach to determining nearshore bathymetry using remotely sensed ocean surface dynamics", *Coastal Engineering* **47**, 265-293.
- Schäffer, H.A.; Madsen, P.A. & Deigaard, R. (1993), "A Boussinesq model for waves breaking in shallow water", *Coastal Engineering* **20**, 185-202.

- Scott, C.P., Cox, D.T., Maddux, T.B., and Long, J.W. (2005). "Large-scale laboratory observations of turbulence on a fixed barred beach", to appear: *Measurement Science and Technology: Special Issue on Water Wave Measurements*, Institute of Physics Publishing, Inc.
- Stockdon, H.F. & Holman, R.A. (2000), "Estimation of wave phase speed and nearshore bathymetry from video imagery", *Journal of Geophysical Research* **105**(C9), 22015-22033.
- Thornton, E.B. & Guza, R.T. (1983), "Transformation of wave height distribution", *Journal of Geophysical Research* **88**(C10), 5925-5938.
- Wei, G.; Kirby, J.T.; Grilli, S.T. & Subramanya, R. (1995), "A fully nonlinear Boussinesq model for surface waves. Part 1. Highly nonlinear unsteady waves", *Journal of Fluid Mechanics* **294**, 71-92.